DFT Study of Formation and Properties of Dinuclear Zirconocene Cations: Effects of Ligand Structure, Solvent, and Metal on the Dimerization Process

Wijitra Meelua[1,2,*], Natchayatorn Keawkla[2], Julianna Oláh[3], and Jitrayut Jitonnom[1]

[1] *Division of Chemistry, School of Science,University of Phayao, Phayao 56000, Thailand*

[2] *Demonstration School, University of Phayao, Phayao 56000, Thailand*

[3] *Department of Inorganic and Analytical Chemistry, Budapest University of Technology and Economics, Gellért tér 4, Budapest H-1111, Hungary*

Corresponding author:
Wijitra Meelua
Phone: +66-5446-6666, Fax: +66-5446-6664,
[*]E-mail: wijitra.me@gmail.com

Abstract

Density functional theory calculations were performed to determine the stability and properties of the formation of dinuclear zirconocene cation $[(Cp_2ZrMe)_2(\mu\text{-}Me)]^+$, a species formed during metallocene/cocatalyst (e.g., $B(C_6F_5)_3$ or MAO) activated polymerization. To improve the catalytic system by minimizing catalyst dimerization, knowledge on the geometric and electronic properties of the process is required. Here, a series of metallocene catalysts were analysed as a function of their ligand structures, solvent and metal. Two different isomers (*cis* and *trans*) of the dimer were considered. The results show that in general the dimer structure in *trans* form is more stable than in the *cis* form. Changing ligand structures tend to destabilize the dimerization process, which is influenced by the steric hindrance on the ligand. The stability of the dimer structure is greatly affected by the choice of solvent polarity, i.e., the more polar solvent the less stability of the dimer. Substitution of Zr into Hf also shows the same trend with a more stable dimer. Vibrational frequencies were calculated for the dimers and the changes in frequencies of the Zr-(μ-Me) stretching vibration were found to correlate well with the dimerization energies (R^2=0.88). Our study might facilitate future catalyst design in metallocene-mediated cationic polymerization.

Keywords: dimerization, cationic polymerization, zirconocene, density functional theory

1. Introduction

Cationic alkyl complexes of Group 4 metallocenes of the type $[Cp_2MR]^+$ (M = Ti, Zr or Hf, Cp = C_5H_5) have been recognized as the catalytically active species in olefin polymerization [1, 2] and cationic polymerization [3] of polar cyclic monomers such as lactones and cyclic carbonates [4-8]. There are relatively few reports for the latter reactions by these catalysts, despite the fact that earlier studies [5, 9-11] have shown that zirconocene complex catalyst can be effective for the cationic ring-opening polymerization (CROP) of cyclic ester monomers. Limited applications of the catalysts in the CROP are probably due to the nature of the cationic process which makes it intrinsically difficult to control the polymer molecular weight [3]. As pointed out by Bochmann [2], generation of cationic polymerization catalysts yields a complex equilibrium of various adducts rather than single-active species.

Recently, a number of experimental studies have been conducted to characterize and/or improve the CROP activity by introducing ligand framework modification to the catalyst structure in combination of different catalytic systems [7, 12]. We have recently utilized density functional theory (DFT) calculations to probe the effects of ligand structure [13-15] and the ring size [6] on the activity of zirconocene-catalyzed CROP, providing atomistic description of all cationic species of the process. These studies focus on the role of ligand structure on the CROP using group 4 metallocene/coctalyst as a catalytic system, which involve the $[Cp_2MR]^+$ compound. However, this highly electron deficient cation may coordinate to the neutral group 4 metallocene compound and this phenomenon is called the dimerization, which reduces the catalyst performance.

In order for the CROP reaction to take place, first the dimethylzirconocene (Cp_2ZrMe_2) compound has to be activated into monomethyl zirconocene (Eq. 1.1) by a cocatalyst (A) such as $B(C_6F_5)_3$ [16, 17] or MAO (methylaluminoxane) which involves the formation of an ion-pair and the subsequent dissociation of the ion-pair to generate a naked cation species (Cp_2ZrMe^+). This cationic species then reacts with either a monomer to yield a polymer (see Eq.1.2) or the catalyst itself to form the dimeric complex having the general formula $[(Cp_2ZrMe)_2(\mu\text{-Me})]^+$ (see Eq. 1.3). The nature of the dimer present in the CROP with metallocene/cocatalyst system is practically difficult to be handled and it contributes to some extent towards the catalyst performance and polymer yield.

$$2\ Cp_2ZrMe_2 + A \rightarrow [Cp_2ZrMe]^+[MeA]^- \rightarrow Cp_2ZrMe^+ + MeA^- \quad (A = MAO \text{ or } B(C_6F_5)_3) \quad (1.1)$$

$$Cp_2ZrMe^+ + Monomer \rightarrow Polymer \quad (1.2)$$

$$Cp_2ZrMe^+ + Cp_2ZrMe_2 \rightarrow [(Cp_2ZrMe)_2(\mu\text{-Me})]^+ \quad (1.3)$$

Evidence for the presence of bridging μ-Me groups in the dimeric structure $[(Cp_2ZrMe)_2(\mu\text{-Me})]^+$ has been reported in the literature by means of NMR studies by several

groups such as Bochmann [18], Brintzinger [19], Tritto [20, 21]. These studies successfully characterized different species in the mixture of dimethylzirconocene and anion cocatalyst (A^- = MAO or $B(C_6F_5)_3$), ($[Cp_2ZrMe]^+$, $[Cp_2ZrMe]^+[MeA]^-$, $[(Cp_2ZrMe)_2(\mu\text{-}Me)]^+[MeA]^-$ and $[(Cp_2ZrMe)_2(\mu\text{-}Me)]^+\cdots\cdots[MeA]^-$. The effect of concentration and conditions on monomer-dimer equilibria was also described. A methylene-bridged complex $[(Cp_2ZrMe)_2(\mu\text{-}CH_2)]$ was also reported [22].

Although the dimer structures have been measured experimentally, detailed theoretical investigations on the dimer formation occurring in the metallocene/cocatalyst polymerization are rather limited, especially how ligand structure influences this process. Klesing et al. was the first to point out that it is possible to predict the substituent pattern that favors complexation of monomers or reduce coordination of any adduct to cationic sites [23]. In particular, they showed that appropriate substituents in 4- and 6-position can minimize the formation of the dimer of a silicon-bridged bisindenyl zirconocene. Vanka et al. [24, 25] reported the DFT studies on the competing process between different species present in the olefin polymerization in solution. Similar study by Zurek et al. [26] was also reported for competitive processes of metallocene/MAO system.

As inspired by the works of Klesing and Vanka, we continue our interest in better understanding the dimer formation occurring in the first step of metallocene-mediated CROP. This kind of information is nowadays limited for polymerization catalyst design. Besides, it is of interest to know how substituents and solvents affect the structure and stability of the catalysis in these reactions. Therefore, we herein describe the effects of the ligand structures on the formation of the dimeric complex $[(Cp_2ZrMe)_2(\mu\text{-}Me)]+$, which were computationally modeled from a set of 38 zirconocene ligands (see Figure 1). The electronic structures and thermal stability of the dimers are then determined according to the analyses of geometric and electronic properties of these ligands. DFT methods have been widely applied in many related studies [6, 15, 27, 28] to provide a detailed description for the chemistry of the cationic ROP process. We also considered the catalytic route (Eq. 1.2) and the deactivation route (see dimerization in Eq. 1.3) as these two are competing processes during the CROP. By studying the dimerization properties of the potential catalysts we intend to provide guidelines for targeted modification of catalysts to enhance the performance of the CROP process.

2. Computational details

To probe the influence of ligand structure on the formation of the dimeric complex (Eq. 1.3), 38 dinuclear zirconocene structures were built and optimized using the initial coordinates reported in the literature [15]. The choices of the catalysts were based on our recent study on the trimethylene carbonate polymerization [14]. In brief, 20 ligands were based on available X-ray crystallographic structures (denoted as C_n) and 18 ligands were computationally modeled here (denoted as H_n) for comparison purposes. For all catalysts in this paper, different ligand orientations around the metal were considered and the most energetically favorable one was selected for geometries and electronic investigations.

Due to the stereochemistry of the dimeric complex, two possible isomers (*cis* and *trans*) of the dimer were considered along the Zr···(μ-Me)···Zr* plane as shown in Figure 2. The difference of the two isomers caused by the orientation of the two zirconocene substructures in the μ-Me complex with respect to each other as a function of their ligand structures. Thus, a total of 76 geometries were generated for the dimers.

It should also be noted that this model is still a slightly crude approximation since, for example, we neglect the interactions between the $B(C_6F_5)_3$ cocatalyst and the dimer. However, it was reported that the formation of zirconocene cation was independent of the cation generating agent such as $B(C_6F_5)_3$ or $[Ph_3C][B(C_6F_5)_4]$ [29]. Furthermore, it was suggested that the inactive Cp_2ZrMe_2 stabilized the $[Cp_2ZrMe]^+$ species more effectively than a solvent molecule or anion coordination [24, 25]. The latter was reported to happen in a weakly non-coordinating anion (i.e., $[(Cp_2ZrMe)_2(\mu\text{-Me})]^+\cdots\cdots[MeA]^-$) [30]. Thus, the cocatalyst was not considered in this study.

DFT calculations were performed using the Gaussian 09 program [31]. Geometries of each species were fully optimized in gas-phase using M06-2X functional [32], which includes the dispersion corrections, and the def2-SVP basis set for all atoms with a 28-electron relativistic effective core potential for Zr or Hf [33]. The basis sets were taken from the EMSL basis set exchange [34]. This M06-2X/def2-SVP method has a widespread application for transition metal complexes [27, 35]. This M06-2X method also proved to be accurate for obtaining dimerization energy of the dimer containing electron-deficient bridges such as μ-Me [36]. Frequency analyses were used to obtain Gibbs free energies (T = 298.15 K, p = 1.013 bar) and to confirm that all located stationary points are minima on the potential energy hypersurface. The solvation model based on density (SMD [37]) as implemented in Gaussian 09, was performed at the same level of theory as the geometry optimization to

compute the molecular properties in solution. Hirshfeld population analysis [38] was used to analyze the charge distribution. Other atomic charges such as Mulliken and NBO were also analyzed (see SI).

The Gibbs free energies for the dimerization or the dimer formation (denoted as ΔG_{dim}) in gas phase and in aqueous solution were estimated by the following equation:

$$\Delta G_{dim} = G(com) - G(pre) - G(cat) \quad (2)$$

where ΔG_{dim} is the free energy change for the dimer formation in Eq. (1), while G(com), G(pre) and G(cat) are Gibbs free-energies for the dimer complex $[(Cp_2ZrMe)_2(\mu\text{-}Me)]^+$ and the two isolated species, i.e., pre-catalyst (Cp_2ZrMe_2) and cationic catalyst (Cp_2ZrMe^+). Thermodynamic properties (energies, enthalpies, and Gibb energies) and vibrational properties of the dimer formation of the studied complexes are provided in the Supporting Information (SI).

For comparison purpose, we also calculated the Gibbs free energies for catalytic route (i.e., initiation/complexation and chain propagation as a rate-determining step [14]) and the results are given in SI, which indicate that there is a correlation between the dimerization energies and the activation energy of the CROP reaction for a series of ligand (see more details in SI).

3. Results and discussion

3.1 Comparison with experiment

Let us first compare the gas-phase and solution structures with the experimental structure of $\{(^{1,2}MeCp)_2ZrMe\}_2(\mu\text{-}Me)^+$ [39], as shown in Table 1. This geometric data indicates that the gas-phase optimized structure of the *trans* dimer $\{(^{1,2}MeCp)_2ZrMe\}_2(\mu\text{-}Me)^+$ is more similar to the X-ray structure than the solution structures. For instance, the *d*(Zr–Zr*) in gas-phase (4.812 Å) is closer to the experimental value (4.821 Å) compared to the same distances in toluene and acetonitrile which yields these Zr–Zr* bond distances longer (4.885 and 5.089 Å, respectively). One can observe that the variations of the geometrical parameters originate from the cationic moiety of the catalyst. For example, when more polar solvent is used the Zr-Zr bond length increases from 4.823 Å in gas phase to 4.877 Å and 5.180 Å in toluene and acetonitrile, respectively. Similarly, *d*(Zr*–μ-Me) increase from 2.463 Å to 2.522 Å in toluene and 2.859 Å in acetonitrile. The angle ∠Cp*Cp* also increases by about 1-6 deg. compared to the corresponding value in gas phase (data not shown). The torsion $\angle CH_3\text{-}Zr\text{-}Zr^*\text{-}CH_3$ is unchanged significantly (≈ 120 deg), as shown in Table 1. Similar dipole moment (μ ≈ 18 D) is seen for both gas phase and solution.

3.2 Relative Stability and Structures of *Cis* and *Trans* Dimer

To understand the effect of ligand structure, it is better to know the important feature of the unsubstituted one. This can be described from the gas-phase structures of the parent catalyst (or C1). The optimized structures of the C1 dimer in the formation of *cis* and *trans* dimers are shown in Figure 2 and their selected geometrical parameters are included in Table 1. As shown, a Me group from Cp_2ZrMe_2 binds to a zirconium atom of Cp_2ZrMe^+ forming a bridging μ-Me group via an intermolecular $Zr^{\cdots}H_3C$ interaction, which is commonly present in metal methyl complexes [18, 19, 40, 41]. For both *cis* and *trans* dimers, the distances are calculated to be ~2.37 and ~2.46 Å for Zr–μ-Me and Zr*–μ-Me, respectively (Figure 2). Hirshfeld charge analysis (Table S2) further indicates that in the dimer complex higher positive charge is delocalised on Zr* atom (qZr*: 0.475-0.517e for *trans* and 0.478-0.520e for *cis*) compared to the Zr one (qZr: 0.459-0.501e for *trans* and 0.457-0.503e for *cis*), whereas these atomic charges become even larger in the isolated species (data not shown). This is in accordance with the the shorter Me-Zr bond in monomeric (avg. d(Zr*–μ) = 2.234 Å) compared to that in dimer (avg. d(Zr–μ) = 2.256 Å).

Table S2 presents the Gibbs free energy of dimerization and selected structural and electronic properties (distance, angle, Hirshfeld charge) of reactant (cation and precatalyst) and product (dimer) species (see Figure 1 for a set of 38 catalyst structures). The formation of the *cis* and *trans* forms is accompanied by similar change in Gibbs free energies (see Table S2; *cis* energies shown in parenthesis). In particular, in the case of 25 out of 38 complexes the *trans* form is more favorable (average ΔG_{dim} = –25.9 kcal/mol), while 13 out of 38 complexes favor the *cis form* (average ΔG_{dim} = –23.8 kcal/mol). Here, it is important to realize that as the formation of the *cis* and *trans* dimers are competing reactions, and the reactant side is the same for them, the obtained differences in dimerization energies are directly related to the relative energies of the *cis* and *trans* forms. Thus, through the example of C1, the dimerization energies are –28.3 kcal/mol for the *trans* form and –26.7 kcal/mol for the *cis* form. This implies that the *cis* form is (-26.7-(-28.3)) = 1.4 kcal/mol higher in energy than the *trans* form. Based on the Bell–Evans–Polanyi principle [42], the transition state for the *cis* form is likely to be only slightly higher for the *trans* form, and we can expect that the dimerization reaction is under thermodynamic control. A relaxed free-energy surface scan was also performed (Figure S6) for the *CH₃-Zr-Zr*-CH₃* dihedral angle in gas-phase at the M06-2X/def2SVP level and it suggests that the *cis* and *trans* isomers are separated by a barrier of 5.5 kcal/mol, in favoring the latter. This, by taking into account the reliability of

our DFT calculations and the Boltzmann distribution of molecules, implies that the reaction mixture contains a mixture of isomers with a larger proportion of *trans* form.

To analyze possible vibration mode that can correlate with the dimerization energies, the vibrational frequencies were computed for the optimized geometries of the zirconocene dimers at the same level as geometry optimizations. A good correlation (R^2 = 0.8864; y=-6.2844x+330.53) between the calculated ΔG_{dim} values and the vibrational frequency of Zr-(μ-Me) bond stretching (Figure 3) for the *trans* dimer is observed. Besides, for Cp_2 ligand the values of ΔG_{dim} grow lineary only when plotting against vibrational frequency of wagging vibration of C-H bond of the μ-Me group with the R^2 value of 0.7 (Figures S7-S8). These results could also be useful as a qualitative descriptor to assess performance trend for the studied dimers.

3.3 Ligand Structure Effect on the Stability of Dimer

Substituent effects on the feasibility of the dimer formation can be predicted with the aid of DFT calculations, as was pointed out by Klesing et al. [23]. However, that work focused on a limited number of substituents and did not study ancillary ligand and/or bridge effects on the process. To further understand how the ligand structure may effect on the dimer formation in Eq. (2), 38 catalysts (Figure 1) were calculated to generate geometric and electronic properties for this dimerization reaction. Such ligand effect was analyzed and discussed through the following ligand substituents, ancillary ligands, and bridge subsections below.

3.3.1 Ligand substituents. We begin with the substituent effects by considering different ligands (Cp or CpInd) substituted by methyl, alkyl, or phenyl groups. Addition of an increasing number of methyl groups to the Cp ring of the ancillary ring ligand (see C1, C3, and H1) destabilizes dimer formation when compared with the unsubstituted Cp by increasing the ΔG_{dim} values from –28.3 kcal/mol in C1 to –25.4 kcal/mol in C3 and –15.9 kcal/mol in H1. A structural change was also observed here, e.g., the ∠CpCp/∠Cp*Cp* angles decrease with increasing steric demand of the ring ligands (48.4°/49.9° in C1 → 45.7°/46.4° in H1). The repulsive interaction within the dimeric complex becomes stronger when adding more methyl group, as can be seen from the increasing of the Zr–Zr distance (*d*(Zr–Zr); 4.823 Å in C1 to 4.840 Å in C3 and 4.996 Å in H1). For linear alkyl chain (see C2 and H2), its length slightly affects the dimer stability of both *trans* (–29.0 *vs*. –28.4 kcal/mol)

and *cis* forms (–25.1 *vs.* –28.9 kcal/mol). Remarkably, this effect is greater for the steric bulky ligand as can be seen by a two-fold increase in the ΔG_{dim} values for C4 compared to C1 (–15.0 *vs.* –28.3 kcal/mol, respectively).

The effect of phenyl substituents can be figured out from CpInd ligand by comparing C14 to H8, H9 and H11. The relative stability of the dimer also depends on the position of the substituent; it decreases in the order H9 (–28.0 kcal/mol) > H8 (–26.8 kcal/mol) > H11 (–23.0 kcal/mol). The latter ligand (H11) shows a poor dimer stability in both *cis* and *trans* isomers (see Table S2), which is attributed to the strong repulsion between the phenyl ring attached to the six-membered ring of the Cp' ligands (see Supplementary).

3.3.2 Ancillary ligand effect. The ancillary effects can be considered by increasing the size of the π-ligands (Cp_2, CpInd, Ind_2 and CpFlu). Extension of the size of the π-ligands leads to the destabilization of the dimer: ΔG_{dim} values becoming less negative (from –28.3 kcal/mol in C1 →–25.6 kcal/mol in C14 → –25.0 kcal/mol in H12 → –19.6 kcal/mol in H15). The same effect is also seen in C3, H7, H17 (from –25.4 to –22.6 and –12.8 kcal/mol, respectively). We also evaluate the electronic effect by reducing the resonance of the Cp' and this effect is smaller compared to the π-ligand size. The electronic effect can further be seen by comparing H12 and H13. It is shown that substitution of the aromatic ring with a saturated one has only a minor destabilizing effect on the dimer formation: (–25.0 *vs.* –23.2 kcal/mol in *trans* and –27.2 *vs.* –25.9 kcal/mol in *cis*). However, this effect becomes greater when adding a double carbon bridge in the Ind as seen in C16 and C17 (–28.0 *vs.* –23.7 kcal/mol in *trans* and –28.8 *vs.* –16.9 kcal/mol in *cis*).

3.3.3 Bridge effect. Finally, we evaluate the bridge effect by comparing the ΔG_{dim} values for the bridge system with respect to the corresponding values for the unbridged system. Table S2 shows that introduction of the bridge ligand mostly stabilizes the dimer formation, as can be seen by the lower ΔG_{dim} values: comparing C1 to C5, C6 (slightly decreasing from –28.3 to –30.0 and –31.1 kcal/mol, respectively) and H1 to C10, C11 (decreasing from –15.9 to –21.9 and –23.0 kcal/mol, respectively) for Cp, H2 to H3 (–28.4 *vs.* –31.1 kcal/mol) for substituted Cp, C14 to C15 (–25.6 *vs.* –26.3 kcal/mol) for mixed CpInd, H12 to H14 (–25.0 *vs.* –24.9 kcal/mol) for Ind_2, and H15 to H16 (–19.6 *vs.* –25.1 kcal/mol) for CpFlu. The data also shows that the type of the bridge atom favors the dimer formation in the order of Ge > Si > C > P for unsubstituted Cp but an opposite trend (Si > Ge) was found for substituted Cp (e.g., C7 *vs.* C8 and C9 *vs.* C10). Apart from its role in influencing the electronic properties

and the stability of the dimer, the bridge significantly affects catalyst geometries. For example, for Cp ligand the bridge tends to increase the CpCp/Cp*Cp* angles (from 48.4°/49.9° in C1 to 58.5°/57.2° in C6) and decrease the CpZrCp/Cp*ZrCp* angles (from 132.8°/133.6° in C1 to 126.1°/126.1° in C6). Similar trend was also found for other ligands (CpFlu, CpInd, Ind_2).

3.4 Solvent Effect on the Stability of Dimer

The polarity of the solvents considerably influences catalytic performance and polymerization yield [1, 43]. However, the role of the solvent on the dimerization is currently unknown. In this section, we aim to know more how solvent influence the stability of the zirconocene dimers (Figure 2). Here, we repeat the geometry optimizations of both monomer and dimer species using an implicit solvent model for toluene and acetonitrile, with the solvent dielectric constants set to ε = 2.374 and 35.688, respectively in the SMD calculations. These solvents are typically used in previous studies using cationic metallocene systems [5, 7, 9, 44].

Figure 4 and Table S8 give the dimerization energies of the selected dimer complexes in toluene and acetonitrile solvents in comparison with the gas-phase energies of the same dimeric complexes. In gas-phase, all the dimerization energies are highly negative showing that the reaction is highly exergonic. One can observe a relevant increase of the dimerization energies when passing from the gas-phase to more polar solvents. This drop is directly attributed to solvent effect that hampers the interaction between the cationic zirconocene and the neutral zirconocene. This solvent effect is more pronounced for acetonitrile. From Figure 4, the dimerization energies of C5 is least affected by the polar solvent, whereas the corresponding energies of C14 is most affected by the polar solvent. It should be noted that the Gibbs free energies for the dimerization process to form the zirconocene dimers are all positive in acetonitrile, which indicates that the formation of these dimers is thermodynamically unfavorable in a polar solvent.

The results clearly suggest that the feasibility of the dimerization strongly depends on the choice of the polar solvent, i.e., the more polar solvent the less stability of the dimer. In this case, acetonitrile is the best solvent among the solvent studied, which may be used to minimize the unwanted resting state species in the metallocene/$B(C_6F_5)_3$ catalytic system.

3.5 Metal Effect on the Stability of Dimer

To probe the metal effect on the dimer formation, we substituted Zr into Hf atom and their structures and energies were recalculated. Here, 12 catalysts showing a linear trend on the plot of Figure 3, i.e., ΔG_{dim} *vs.* ν(Zr-μ-Me), were selected to probe this effect. The results shown in Table S12 indicate that the stability of the dimer structures are higher (i.e., more negative ΔG_{dim} value), the distance between the metal (M-M; M=Zr or Hf) become shorter, and the Hirshfeld charge distributions on the metal atom slightly increase when replacing Zr with Hf.

Conclusion

A detailed DFT analysis of the formation of dimeric product $[(Cp_2ZrMe)_2(\mu\text{-Me})]^+$ formed by the cationic and neutral species of zirconocene was performed for a set of different catalyst structures (Figure 2) and their relative stabilities and relevant properties were evaluated. Two different configurations (*cis* and *trans*) on the dimer complex were considered. The effect of ligand structure on the stability and related properties during the formation of dimeric complex was systematically analyzed for 38 zirconocene complexes (Figure 3). The *trans* isomers are dominated by the number over the *cis* one but both trans and *cis* complexes are close in energy to each other, which can be readily converted to one another at room temperature. We found a linear correlation (R^2=0.88) between the ΔG_{dim} values for *trans* form and the vibrational frequency of the Zr-(μ-Me) stretching vibration. Calculations indicate that modifying ligand structures tend to destabilize the complex in both isomers. The results of the solvent effect in Figure 4 shows that the dimerization is quite disfavor process in acetonitrile but it is a spontaneous process in both the gas phase and toluene. For metal effect, changing Zr to Hf tends to give a more stable dimer structure (Hf is more stable by *ca.* 1.5 kcal/mol). Thus, it is clear that the dimerization can be minimized in a more polar solvent, which can be used to promote efficient catalyst performance.

Acknowledgements

J.J. and W.M. would like to thank the Demonstration School University of Phayao and the SCiUS Project (http://scius.most.go.th/) Students (Chanita Techotanont, Naphutsaporn Wongsamart, and Worachit Wannasompon) for their supports. Financial supports by the University of Phayao (Grant RD62042) and the Thailand Research Fund (Grant RSA6280104) are gratefully acknowledged. J.O. was supported by NKFIH Grant No. 115503.

References

[1] R.A. Collins, A.F. Russell, P. Mountford, Group 4 metal complexes for homogeneous olefin polymerisation: a short tutorial review, Appl. Petrochem. Res. 5(3) (2015) 153-171.
[2] M. Bochmann, Cationic Group 4 metallocene complexes and their role in polymerisation catalysis: the chemistry of well defined Ziegler catalysts, J. Chem. Soc., Dalton Trans. (3) (1996) 255-270.
[3] Y. Sarazin, J.-F. Carpentier, Discrete cationic complexes for ring-opening polymerization catalysis of cyclic esters and epoxides, Chem. Rev. 115(9) (2015) 3564-3614.
[4] T. Endo, Y. Shibasaki, F. Sanda, Controlled ring-opening polymerization of cyclic carbonates and lactones by an activated monomer mechanism, J. Polym. Sci. A Polym. Chem. 40(13) (2002) 2190-2198.
[5] M. Hayakawa, M. Mitani, T. Yamada, T. Mukaiyama, Living ring-opening polymerization of lactones using cationic zirconocene complex catalysts, Macromol. Chem. Phys. 198(5) (1997) 1305-1317.
[6] J. Jitonnom, W. Meelua, Cationic ring-opening polymerization of cyclic carbonates and lactones by group 4 metallocenes: A theoretical study on mechanism and ring-strain effects, J. Theor. Comput. Chem. 16(1) (2017) 1750003.
[7] K. Kostakis, S. Mourmouris, G. Karanikolopoulos, M. Pitsikalis, N. Hadjichristidis, Ring-opening polymerization of lactones using zirconocene catalytic systems: Block copolymerization with methyl methacrylate, J. Polym. Sci. A Polym. Chem. 45(16) (2007) 3524-3537.
[8] A. Valente, P. Zinck, A. Mortreux, M. Visseaux, P.J.G. Mendes, T.J.L. Silva, M.H. Garcia, Polymerization of ε-caprolactone using ruthenium(II) mixed metallocene catalysts and isopropyl alcohol: Living character and mechanistic study, J. Mol. Catal. A: Chem. 346(1–2) (2011) 102-110.
[9] M. Hayakawa, M. Mitani, T. Yamada, T. Mukaiyama, Living ring-opening polymerization of cyclic carbonate using cationic zirconocene complex as catalyst, Macromol. Rapid Commun. 17(12) (1996) 865-870.
[10] Z. Ariffin, D. Wang, Z. Wu, Synthesis of polycarbonates using a cationic zirconocene complex, Macromol. Rapid Commun. 19(12) (1998) 601-604.
[11] T. Mukaiyama, M. Hayakawa, K. Oouchi, M. Mitani, T. Yamada, Preparation of narrow polydispersity polycaprolactone catalyzed by cationic zirconocene complexes, Chem. Lett. 24 (1995) 737-738.
[12] E. Villaseñor, R. Gutierrez-Gonzalez, F. Carrillo-Hermosilla, R. Fernández-Galán, I. López-Solera, A.R. Fernández-Pacheco, A. Antiñolo, Neutral dimethylzirconocene complexes as initiators for the ring-opening polymerization of ε-caprolactone, Eur. J. Inorg. Chem. 2013(7) (2013) 1184-1196.
[13] J. Jitonnom, W. Meelua, Effects of silicon-bridge and π-ligands on the electronic structures and related properties of dimethyl zirconocene polymerization catalysts: a comparative theoretical study, Chiang Mai J. Sci. 41(5.2) (2014) 1220-1229.
[14] J. Jitonnom, W. Meelua, Effect of ligand structure in the trimethylene carbonate polymerization by cationic zirconocene catalysts: A “naked model” DFT study, J. Organomet. Chem. 841 (2017) 48-56.
[15] J. Jitonnom, W. Meelua, Data on electronic structures for the study of ligand effects on the zirconocene-mediated trimethylene carbonate polymerization, Data in Brief 20 (2018) 1867-1869.

[16] E.Y.-X. Chen, T.J. Marks, Cocatalysts for metal-catalyzed olefin polymerization: Activators, activation processes, and structure-activity relationships, Chem. Rev. 100(4) (2000) 1391-1434.
[17] M. Bochmann, The chemistry of catalyst activation: the case of group 4 polymerization catalysts, Organometallics 29(21) (2010) 4711-4740.
[18] M. Bochmann, S.J. Lancaster, Monomer-dimer equilibria in homo- and heterodinuclear cationic alkylzirconium complexes and their role in polymerization catalysis, Angew. Chem. Int. Ed. Engl. 33(15-16) (1994) 1634-1637.
[19] S. Beck, M.-H. Prosenc, H.-H. Brintzinger, R. Goretzki, N. Herfert, G. Fink, Binuclear zirconocene cations with μ-CH3-bridges in homogeneous Ziegler-Natta catalyst systems, J. Mol. Catal. A-Chem. 111(1) (1996) 67-79.
[20] I. Tritto, R. Donetti, M.C. Sacchi, P. Locatelli, G. Zannoni, Dimethylzirconocene-methylaluminoxane catalyst for olefin polymerization: NMR study of reaction equilibria, Macromolecules 30(5) (1997) 1247-1252.
[21] I. Tritto, R. Donetti, M.C. Sacchi, P. Locatelli, G. Zannoni, Evidence of zircononium−polymeryl ion pairs from 13C NMR in situ 13C2H4 polymerization with Cp2Zr(13CH3)2-based catalysts, Macromolecules 32(2) (1999) 264-269.
[22] M. Hogenbirk, G. Schat, Otto S. Akkerman, F. Bickelhaupt, J. Schottek, M. Albrecht, R. Fröhlich, G. Kehr, G. Erker, H. Kooijman, Anthony L. Spek, (μ-Methylene)bis(methylzirconocene): preparation, molecular structure, and thermal disproportionation, Eur. J. Inorg. Chem. 2004(6) (2004) 1175-1182.
[23] A. Klesing, S. Bettonville, The effect of substituents on dimer formation and cation–anion interaction in silicon bridged bisindenyl zirconocene propylene polymerization catalysts, Physical chemistry chemical physics : PCCP 1(9) (1999) 2373-2377.
[24] K. Vanka, M.S.W. Chan, C.C. Pye, T. Ziegler, Exploring the activation of olefin polymerisation catalysts with density functional theory, Macromolecular Symposia 173(1) (2001) 163-178.
[25] K. Vanka, T. Ziegler, A density functional study of the competing processes occurring in solution during ethylene polymerization by the catalyst (1,2-Me2Cp)2ZrMe+, Organometallics 20(5) (2001) 905-913.
[26] E. Zurek, T. Ziegler, Toward the identification of dormant and active species in MAO (methylaluminoxane)-activated, dimethylzirconocene-catalyzed olefin polymerization, Organometallics 21(1) (2002) 83-92.
[27] A. Laine, B.B. Coussens, J.T. Hirvi, A. Berthoud, N. Friederichs, J.R. Severn, M. Linnolahti, Effect of ligand structure on olefin polymerization by a metallocene/borate catalyst: a computational study, Organometallics 34(11) (2015) 2415-2421.
[28] J. Sassmannshausen, Computational studies of the unusual water adduct [$Cp_2TiMe(OH_2)$](+): the roles of the solvent and the counterion, Dalton Trans. 43(29) (2014) 11195-201.
[29] J. Saßmannshausen, Cationic and dicationic zirconocene compounds as initiators of carbocationic isobutene polymerisation, Dalton transactions (41) (2009) 9026-9032.
[30] E.P. Talsi, J.L. Eilertsen, M. Ystenes, E. Rytter, 1H-NMR spectroscopic study of cationic intermediates in solvent and oil constituents of the catalytic systems Cp2ZrMe2/[CPh3][B(C6F5)4] and Cp2ZrMe2/AlMe3/[CPh3][B(C6F5)4] in benzene, J. Organomet. Chem. 677(1) (2003) 10-14.
[31] G.W.T. M. J. Frisch, H. B. Schlegel, G. E. Scuseria, M. A. Robb, J. R. Cheeseman, G. Scalmani, V. Barone, B. Mennucci, G. A. Petersson, H. Nakatsuji, M. Caricato, X. Li, H. P. Hratchian, A. F. Izmaylov, J. Bloino, G. Zheng, J. L. Sonnenberg, M. Hada, M. Ehara, K. Toyota, R. Fukuda, J. Hasegawa, M. Ishida, T. Nakajima, Y. Honda, O. Kitao, H. Nakai, T. Vreven, J. A. Montgomery, Jr., J. E. Peralta, F. Ogliaro, M. Bearpark, J. J. Heyd, E. Brothers,

K. N. Kudin, V. N. Staroverov, T. Keith, R. Kobayashi, J. Normand, K. Raghavachari, A. Rendell, J. C. Burant, S. S. Iyengar, J. Tomasi, M. Cossi, N. Rega, J. M. Millam, M. Klene, J. E. Knox, J. B. Cross, V. Bakken, C. Adamo, J. Jaramillo, R. Gomperts, R. E. Stratmann, O. Yazyev, A. J. Austin, R. Cammi, C. Pomelli, J. W. Ochterski, R. L. Martin, K. Morokuma, V. G. Zakrzewski, G. A. Voth, P. Salvador, J. J. Dannenberg, S. Dapprich, A. D. Daniels, O. Farkas, J. B. Foresman, J. V. Ortiz, J. Cioslowski, and D. J. Fox Gaussian 09, Revision A.02; Gaussian, Inc.: Wallingford, CT, 2009.

[32] Y. Zhao, D.G. Truhlar, The M06 suite of density functionals for main group thermochemistry, thermochemical kinetics, noncovalent interactions, excited states, and transition elements: two new functionals and systematic testing of four M06-class functionals and 12 other functionals, Theor. Chem. Acc. 120(1) (2008) 215-241.

[33] D. Andrae, U. Häußermann, M. Dolg, H. Stoll, H. Preuß, Energy-adjusted ab initio pseudopotentials for the second and third row transition elements, Theor. Chim. Acta 77(2) (1990) 123-141.

[34] K.L. Schuchardt, B.T. Didier, T. Elsethagen, L. Sun, V. Gurumoorthi, J. Chase, J. Li, T.L. Windus, Basis set exchange: a community database for computational sciences, J. Chem. Inf. Model. 47(3) (2007) 1045-1052.

[35] H. Goossens, S. Catak, M. Glassner, V.R. de la Rosa, B.D. Monnery, F. De Proft, V. Van Speybroeck, R. Hoogenboom, Cationic ring-opening polymerization of 2-propyl-2-oxazolines: Understanding structural effects on polymerization behavior based on molecular modeling, ACS Macro Lett. 2(8) (2013) 651-654.

[36] C. Ehm, G. Antinucci, P.H.M. Budzelaar, V. Busico, Catalyst activation and the dimerization energy of alkylaluminium compounds, J. Organomet. Chem. 772-773 (2014) 161-171.

[37] A.V. Marenich, C.J. Cramer, D.G. Truhlar, Universal solvation model based on solute electron density and on a continuum model of the solvent defined by the bulk dielectric constant and atomic surface tensions, J. Phys. Chem. 113(18) (2009) 6378-6396.

[38] F.L. Hirshfeld, Bonded-atom fragments for describing molecular charge densities, Theor. Chim. Acta 44(2) (1977) 129-138.

[39] L. Li, T.J. Marks, New organo-lewis acids. tris(β-perfluoronaphthyl)borane (PNB) as a highly active cocatalyst for metallocene-mediated Ziegler−Natta α-olefin polymerization, Organometallics 17(18) (1998) 3996-4003.

[40] M.J. Ingleson, A. Clarke, M.F. Mahon, J.P. Rourke, A.S. Weller, [Cp2ZrMe(12-μ-Me-1-closo-CB11HMe10)]: a transition metal complex of a highly-methylated carborane anion, Chem. Commun. (15) (2003) 1930-1931.

[41] O. Eisenstein, Y. Jean, Factors favoring an M...H-C interaction in metal-methyl complexes. An MO analysis, J. Am. Chem. Soc. 107(5) (1985) 1177-1186.

[42] R. Bruckner, Advanced Organic Chemistry, Harcourt/Academic Press, Chapter 1, Burlington, Mass, 2002.

[43] L. Castro, E. Kirillov, O. Miserque, A. Welle, L. Haspeslagh, J.-F. Carpentier, L. Maron, Are solvent and dispersion effects crucial in olefin polymerization DFT calculations? some insights from propylene coordination and insertion reactions with group 3 and 4 metallocenes, ACS Catal. 5(1) (2015) 416-425.

[44] M.-E. Kourti, E. Fega, M. Pitsikalis, Block copolymers based on 2-methyl- and 2-phenyl-oxazoline by metallocene-mediated cationic ring-opening polymerization: synthesis and characterization, Polym. Chem. 7(16) (2016) 2821-2835.

[45] J.L. Eilertsen, J.A. Støvneng, M. Ystenes, E. Rytter, Activation of metallocenes for olefin polymerization as monitored by IR spectroscopy, Inorg. Chem. 44(13) (2005) 4843-4851.

Table and Figure legends

Table 1. Computed bond lengths (Å), angles (°), dipole moment (μ) of $[\{(^{1,2}MeCp)_2ZrMe\}_2(\mu\text{-}Me)]^+$ and $[(Cp_2ZrMe)_2(\mu\text{-}Me)]^+$ (C1) in *trans* form. Calculated and experimental vibrational frequencies (ν, cm^{-1}) of out-of-plane deformation of the C-H bonds of the Cp ring are also included for C1.

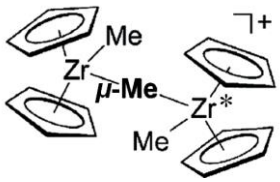

	$[\{(^{1,2}MeCp)_2ZrMe\}_2(\mu\text{-}Me)]^+$				$[(Cp_2ZrMe)_2(\mu\text{-}Me)]^+$			
Parameters	*Expt.*[a]	*Gas*	*Toluene*	*Acetonitrile*	*Expt.*[b]	*Gas*	*Toluene*	*Acetonitrile*
d(Zr–Zr*)	4.821	4.812	4.885	5.089	-	4.823	4.877	5.180
d(Zr–μ-Me)	2.405	2.366	2.374	2.344	-	2.367	2.369	2.332
d(Zr*–μ-Me)	2.432	2.475	2.527	2.760	-	2.463	2.522	2.859
d(Zr–Me)	2.255	2.253	2.258	2.292	-	2.250	2.269	2.303
d(Zr*–Me)	2.235	2.244	2.260	2.292	-	2.245	2.260	2.290
∠Zr–(μ-Me)–Zr*	170.9	167.5	170.6	171.1	-	173.7	171.1	172.5
∠(μ-Me)–Zr–Me	92.0	91.5	90.9	86.0	-	91.8	90.3	86.2
∠(μ-Me)–Zr*–Me	93.7	92.6	92.9	95.4	-	92.1	93.8	97.6
μ	-	17.503	17.181	16.419	-	18.279	18.309	17.999
$\nu(cm^{-1})$					818 (803)	842 (821)	821 (816)	819 (797)

[a] Taken from Ref [39].

[b] Frequency of out-of-plane deformation of the C-H bonds of the Cp ring for $[(Cp_2ZrMe)_2(\mu\text{-}Me)]^+$ and Cp_2ZrMe_2 (shown in parenthesis) which was taken from Ref [45].

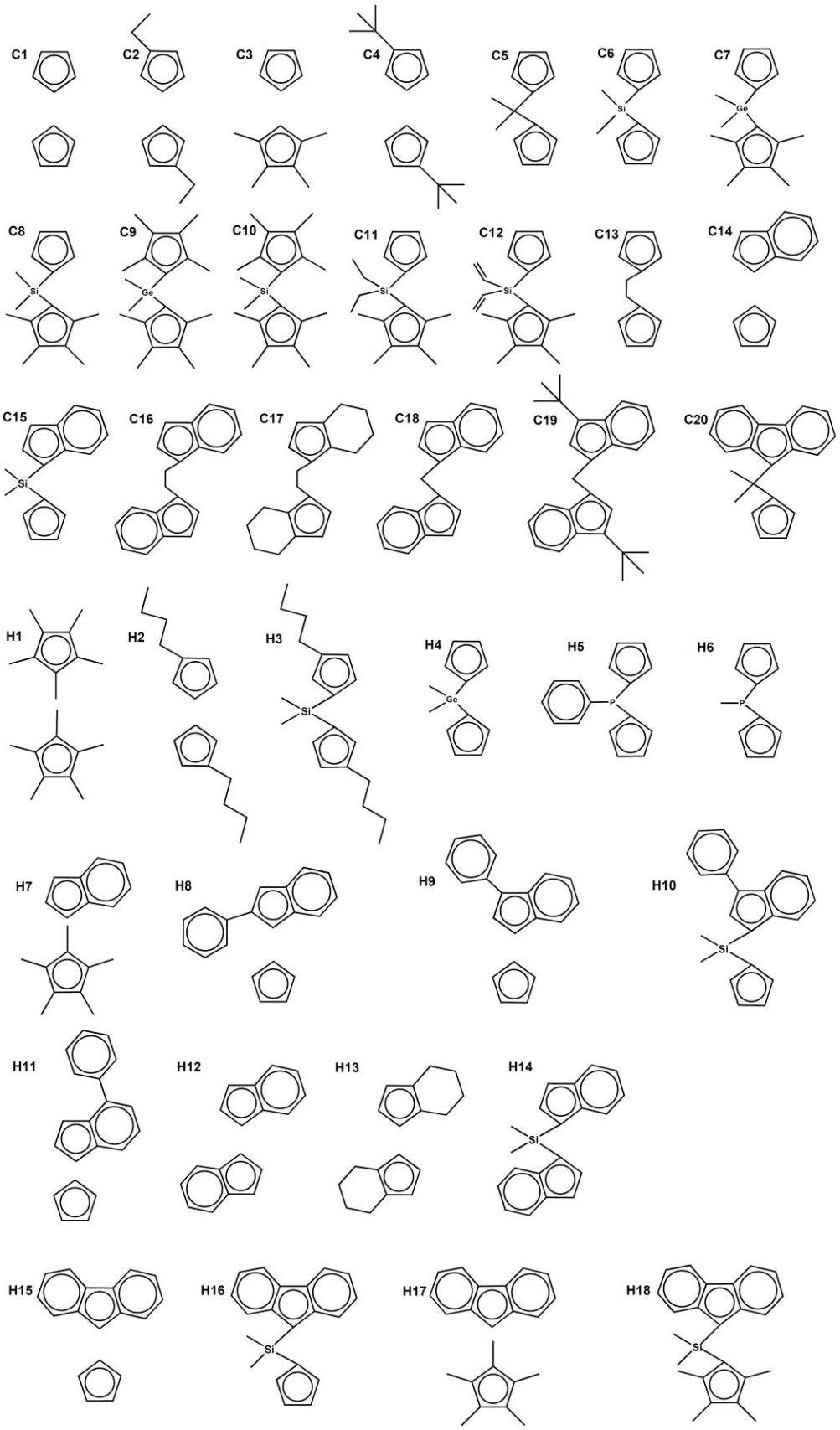

Figure 1. Schematic ligand structures of the studied zirconocenes.

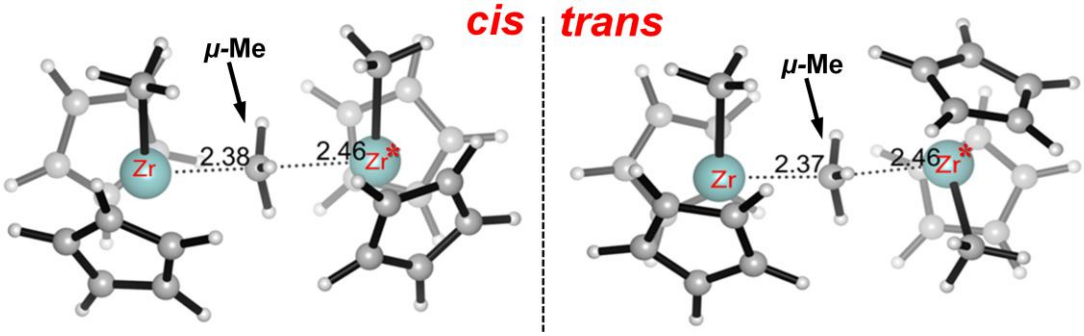

Figure 2. Possible *cis/trans* isomers of the dimeric complex $[Cp_2ZrMe_2(\mu\text{-}Me)]^+$.

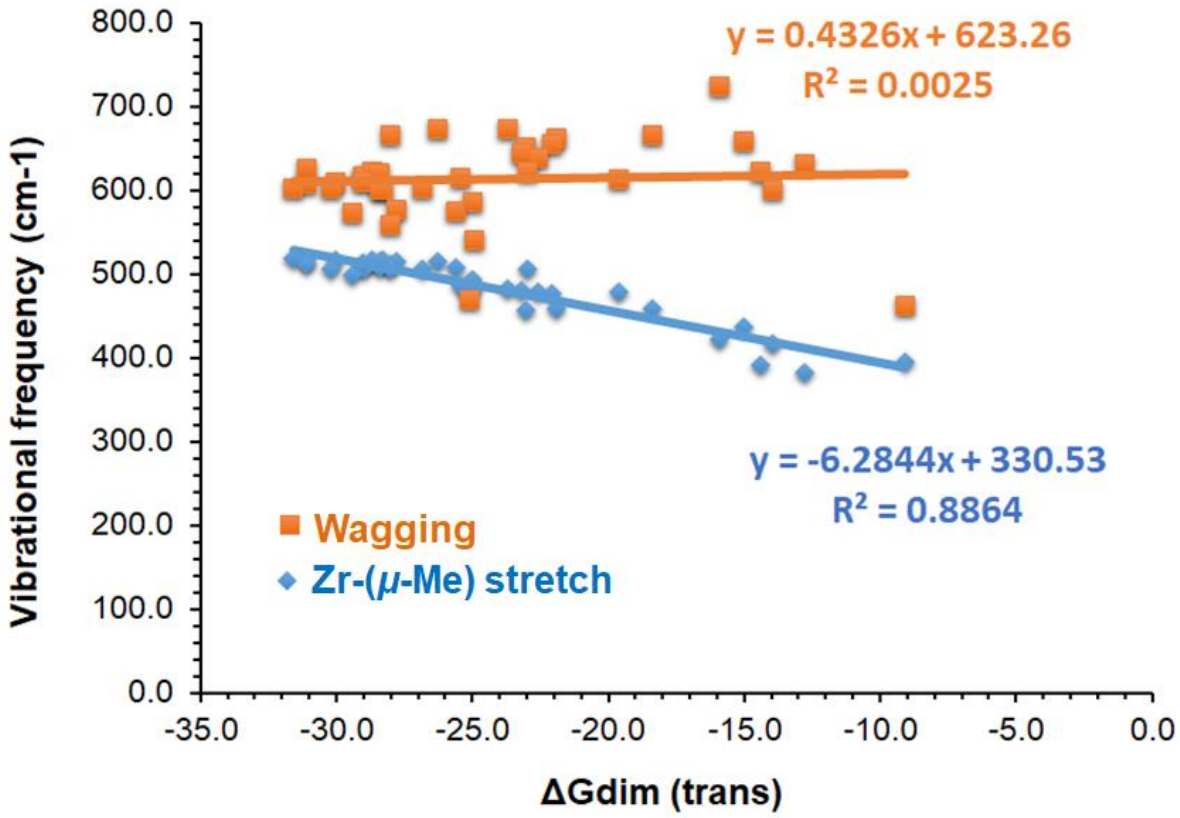

Figure 3. Plot of linear correlation between ΔG_{dim} (trans) and the vibrational frequencies (cm^{-1}) of two vibrations (wagging and Zr-(μ-Me) stretch) at μ-Me position (see also Figure S7).

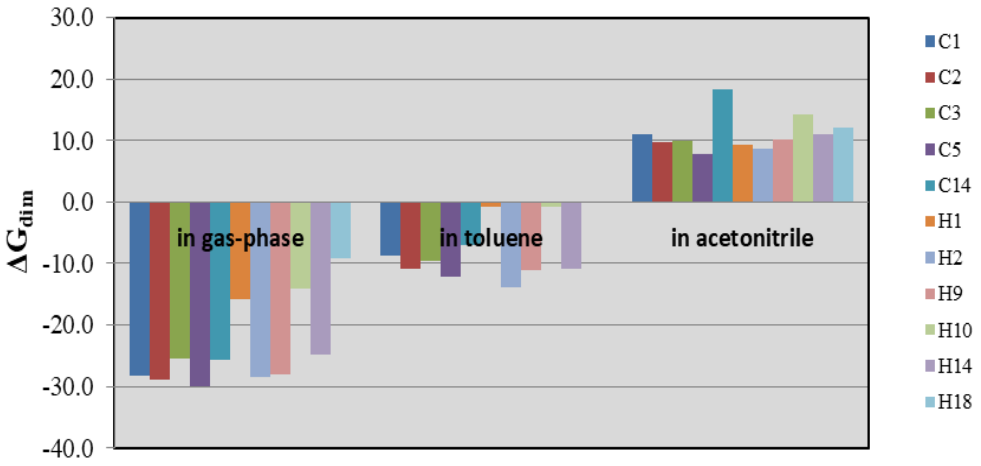

Figure 4. Effect of solvent on the ΔG_{dim} values (in kcal/mol) for selected ligands